ACS APPLIED MATERIALS & INTERFACES

Research Article

www.acsami.org

Entropy-Driven Conformational Control of α,ω-Difunctional Bidentate-Dithiol Azo-Based Adsorbates Enables the Fabrication of Thermally Stable Surface-Grafted Polymer Films

Han Ju Lee, Andrew C. Jamison, and T. Randall Lee*

Department of Chemistry and the Texas Center for Superconductivity, University of Houston, 4800 Calhoun Road, Houston, Texas 77204-5003, United States

Supporting Information

ABSTRACT: Thermally stable radical initiator monolayers were prepared from uniquely designed α,ω-difunctional adsorbates with bidentate headgroups for the growth of nanoscale polymer films on metal surfaces. The length of the spacer separating the bidentate headgroups was varied to afford 4,4′-(diazene-1,2-diyl)bis(*N*-(16-(3,5-bis(mercaptomethyl)phenoxy)hexadecyl)-4-cyanopentanamide) (**B16**), 4,4′-(diazene-1,2-diyl)bis(*N*-(16-(3,5-bis(mercaptomethyl)phenoxy)decyl)-4-cyanopentanamide) (**B10**), and 4,4′-(diazene-1,2-diyl)bis(*N*-(4-(3,5-bis(mercaptomethyl)phenoxy)-butyl)-4-cyanopentanamide) (**B4**). The structural features of the self-assembled monolayers (SAMs) derived from **B16**, **B10**, and **B4** were characterized by X-ray photoelectron spectroscopy (XPS), ellipsometry, and polarization modulation infrared reflection−absorption spectroscopy (PM-IRRAS) and compared to those derived from an analogous α,ω-difunctional adsorbate with monodentate headgroups, 4,4′-(diazene-1,2-diyl)bis(4-cyano-*N*-(16-mercaptohexadecyl)pentanamide (**M**). These studies demonstrate that the conformation (i.e., hairpin vs standing up) of the bidentate initiator adsorbates on gold surfaces was easily controlled by adjusting the concentration of the adsorbates in solution. The results of solution-phase thermal desorption tests revealed that the radical initiator monolayers generated from **B16**, **B10**, and **B4** exhibit an enhanced thermal stability when compared to those generated from **M**. Furthermore, a study of the growth of polymer films was performed to evaluate the utility of these new bidentate adsorbate SAMs as film-development platforms for new functional materials and devices. Specifically, surface-grafted polystyrene films were successfully generated from SAMs derived from **B16**. In contrast, attempts to grow polystyrene films from SAMs derived from **M** under a variety of analogous conditions were unsuccessful.

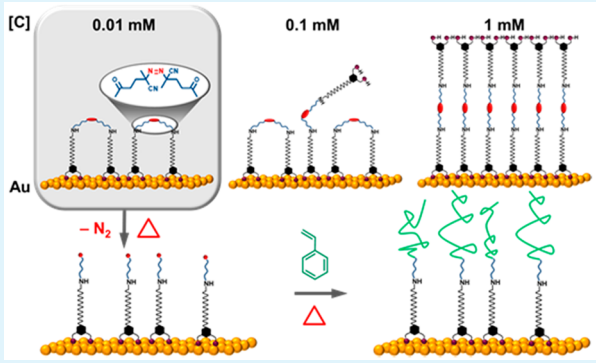

KEYWORDS: *surface-grafted polymerization, radical initiator, self-assembled monolayers, polymer films, multidentate, thermal stability*

INTRODUCTION

The evolution of surface-grafted polymer technologies over the last three decades has allowed the development of nanoscale sensors,[1−4] photovoltaic cells,[5,6] antifouling coatings,[7−9] and patterned platforms to fabricate a host of new nano- and microsized devices.[10−16] Thin polymer films prepared by surface-initiated polymerization offer several advantages.[17,18] First, such polymeric thin films can be generated on curved surfaces, such as the surfaces of nanoparticles, as well as on flat surfaces. Second, the thickness of the films can be controlled on the scale of angstroms. Third, the stability of polymer coatings grafted on surfaces via chemical bonds is greater than that of polymer coatings attached via physical adsorption. Finally, surface grafting allows facile control over the surface concentration of polymer initiators and thus precise control over the density of the resultant polymer chains.

Surface-immobilized initiators allow the growth of polymer chains directly from surfaces. The types of headgroups used to bind initiator moieties to surfaces depend on the nature of the bonding sites and/or the functional groups on the surface. Initiator adsorbates having trialkoxysilane headgroups are used to form monolayers on metal oxide surfaces, such as silicon oxide and indium tin oxide (ITO), via strong Si−O linkages.[2,5,7,8,10] In contrast, initiator adsorbates having thiol or disulfide headgroups are used to generate monolayers on *gold* surfaces,[3,4,9,12−16,19−27] leading to advanced applications in fields ranging from molecular electronics to biosensing.[28−30] Notably, however, Au−S bonds are more labile than Si−O bonds at elevated temperatures and at high concentrations of radical species, which limits the use of organosulfur adsorbates as platforms for the growth of polymer films. Several research groups have reported strategies for enhancing the stability of

Received: February 17, 2016
Accepted: May 24, 2016
Published: May 24, 2016

DOI: 10.1021/acsami.6b02025
ACS Appl. Mater. Interfaces 2016, 8, 15691−15699

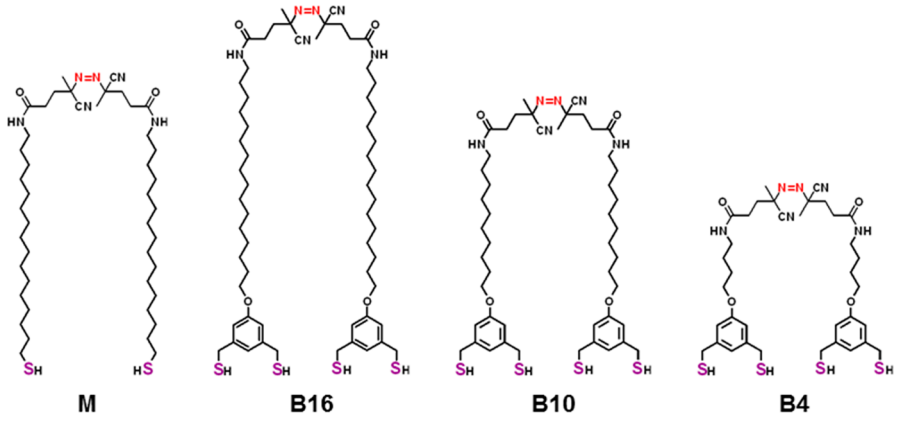

Figure 1. Structures of the radical initiator adsorbates examined in this report.

organosulfur adsorbates on gold surfaces during thermal radical polymerizations. Shah and co-workers used radical initiator monolayers generated from $(BrC(CH_3)_2COO(CH_2)_{10}S)_2$ at 60 °C for surface-initiated polymerization.[12] The stability of these initiator monolayers was sufficient to grow patterned polymer brushes on gold substrates. Additionally, cross-linked poly(siloxane) layers have been used to provide thermal and chemical stability to thiol-based initiator monolayers.[23−25] Huang and co-workers prepared thermally stable radical initiator monolayers by incorporating such cross-linked poly(siloxane) layers between thiolates, exposing termini that consisted of azobis(isobutyronitrile) (AIBN) moieties.[23] For this system, cross-linked thiol initiator layers on gold surfaces showed the same thermal stability as silane initiator layers on silicon oxide surfaces for the growth of polystyrene films. While the aforementioned two methods provided stable initiator monolayers for the growth of polymer films, these procedures required multiple surface adsorption/modification steps rather than a single surface adsorption step that is characteristic of the formation of self-assembled monolayers (SAMs).

AIBN-containing monolayers are ubiquitous in surface-initiated polymerizations.[7,14,15,23,26,27,31,32] For a typical AIBN-initiator monolayer, one end of the AIBN moiety is bound to a surface-attached adsorbate, while the other end is aligned toward the solution. When activated under heat or light, AIBN generates two radicals that can instigate polymerization. One of these radicals is tethered from the surface and participates in surface-initiated polymerization; however, the other radical fragment is unbound and generates free polymers in solution. These unbound polymers frequently adhere to the bound polymer film and can typically be removed by washing with an appropriate solvent, but polymer shells mixed with silica− or metal−polymer core−shell nanoparticles cannot be separated easily. To solve this problem, Czaun and co-workers used α,ω-difunctional silane adsorbates having an AIBN moiety *between* the silane headgroups to form a hairpin conformation for the initiator adsorbate on silicon oxide surfaces.[32] In this system, the polymer chains grew only from the surfaces since all chain-forming radicals were tethered. Similarly, α,ω-dithiol adsorbates having an AIBN moiety were examined by Dyer's group for grafting polymers on gold surfaces.[14,15] However, these studies never sought to prepare radical initiator monolayers composed of surface-bound adsorbates in the hairpin conformation.

With the aforementioned results in mind, we designed and synthesized a new class of radical initiator adsorbate for fabricating surface-grafted polymer thin films on metal surfaces. Our adsorbate design features two unique structural characteristics: (1) a dithiol headgroup to enhance thermal and radical stability,[33,34] and (2) an α,ω-difunctional architecture to immobilize all of the initial AIBN radical polymerization sites.[32] Prior work by our group[34] has demonstrated the value of chelating headgroups for entropically favored surface bonding; however, our new difunctional adsorbates add a second dimension to the "chelate effect" by enabling similar proximity dynamics to generate surface attachments from the unbound ends of these chains, in competition with adsorbates in solution. The new adsorbates are 4,4′-(diazene-1,2-diyl)bis(*N*-(16-(3,5-bis(mercaptomethyl)phenoxy)hexadecyl)-4-cyanopentanamide) (**B16**), 4,4′-(diazene-1,2-diyl)bis(*N*-(16-(3,5-bis(mercaptomethyl)phenoxy)decyl)-4-cyanopentanamide) (**B10**), and 4,4′-(diazene-1,2-diyl)bis(*N*-(4-(3,5-bis(mercaptomethyl)phenoxy)butyl)-4-cyanopentanamide) (**B4**), shown in Figure 1. Herein, we examine the structural features and thermal stability of the initiator-tethered SAMs generated from the bisbidentate adsorbates **B16**, **B10**, and **B4**, comparing their properties to those generated from an analogous α,ω-difunctional adsorbate with monodentate headgroups: 4,4′-(diazene-1,2-diyl)bis(4-cyano-*N*-(16-mercaptohexadecyl)-pentanamide (**M**). Specifically, we generated initiator monolayers from three different concentrations (0.01, 0.1, and 1 mM) of each adsorbate solution to examine the effect of concentration on the conformation (hairpin vs standing up) of the adsorbates within the monolayers formed on gold surfaces. Furthermore, we describe the results of a comparative study between **B16** and **M** monolayers for generating surface-grafted polystyrene on gold.

EXPERIMENTAL SECTION

Complete details regarding the materials, procedures, and instrumentation used to conduct the research reported here are provided in the Supporting Information.

RESULTS AND DISCUSSION

I. Impact of Concentration of Adsorbate Solutions on Radical Initiator Surface Bonding. Evaporated gold slides were immersed in THF solutions (0.01, 0.1, and 1 mM) of **M**, **B16**, **B10**, and **B4** for 48 h at room temperature (rt). The resultant SAMs were characterized by XPS, ellipsometry, and PM-IRRAS.

XPS Analysis of Radical Initiator Monolayers on Flat Gold Surfaces. A well-known approach to determining the relative degree of bonding of the sulfur moieties to gold in

DOI: 10.1021/acsami.6b02025
ACS Appl. Mater. Interfaces 2016, 8, 15691−15699

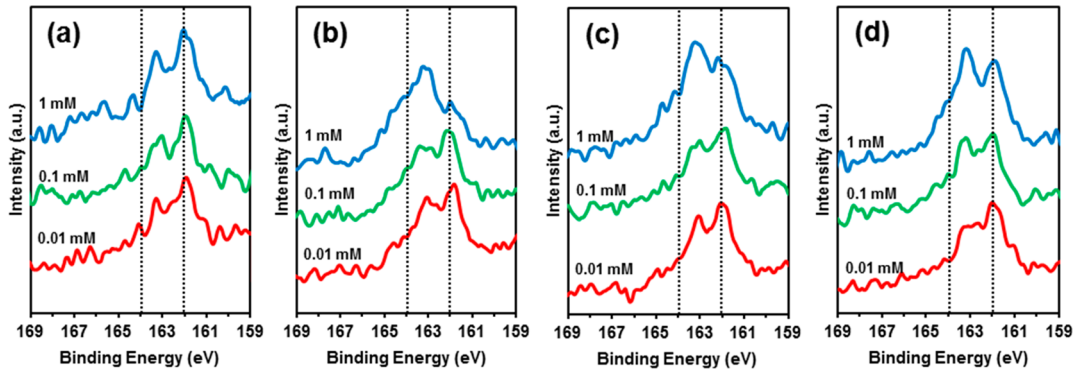

Figure 2. XPS S 2p spectra of the films generated at 0.01, 0.1, and 1 mM from (a) **M**, (b) **B16**, (c) **B10**, and (d) **B4** in THF. Dashed lines provide a means of identifying peaks associated with bound thiolate (~162 eV) and unbound thiol or disulfides (~164 eV).

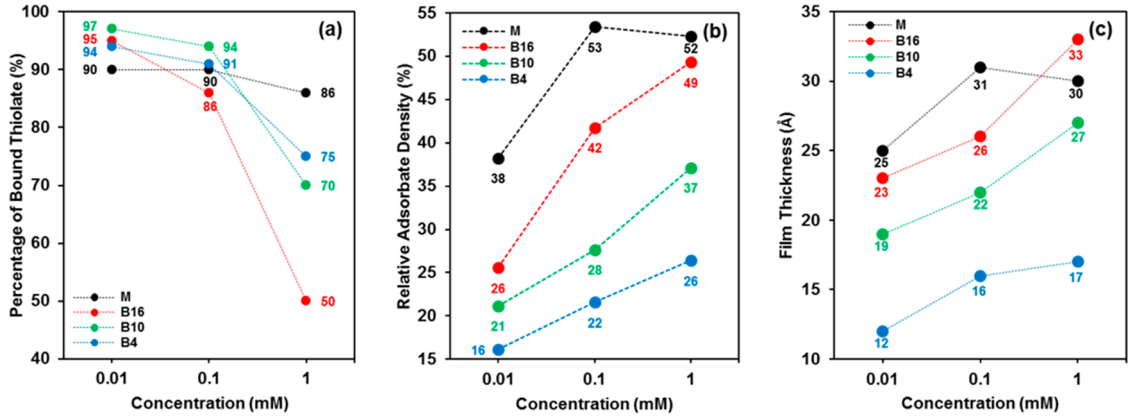

Figure 3. (a) Percentages of bound thiolate, (b) relative adsorbate density profiles, and (c) film thickness profiles of the indicated radical initiator monolayers as a function of deposition solution concentration. The percentages of bound thiolate were obtained by deconvolution of the XPS S 2p spectra. The adsorbate density percentages were determined in comparison to the ratio of S/Au for the monolayer formed from **C18SH** (0.0106), assuming the adsorbate density of the **C18SH** film to be 100%. In a comparison with **C18SH**, the S/Au ratio for **M** was divided by a factor of 2, while those of **B16**, **B10**, and **B4** were divided by a factor of 4. The reproducibilities of the percentages of bound thiolate, relative adsorbate density, and ellipsometric thickness were within ±2%, ±2%, and ±2 Å, respectively.

thioadsorbate films is through the analysis of the peaks in the S 2p region of the X-ray photoelectron spectra.[35] Peaks at 162.0 and 163.2 eV with a 2:1 integrated peak area ratio are associated with S $2p_{3/2}$ and S $2p_{1/2}$ for bound thiolate on gold, respectively, while the S $2p_{3/2}$ peak for unbound thiol or disulfide appears at ~163.5−164 eV, with the S $2p_{1/2}$ peak ~1.2 eV higher in energy. On the basis of these values, we used the spectra in Figure 2 to determine the degree to which the adsorbates were bound to gold. The XPS S 2p spectra for the radical initiator monolayers generated from the bidentate adsorbates (**B16**, **B10**, and **B4**) show similar trends in relative peak intensities (~162 eV versus ~164 eV) for the various concentrations of adsorbate deposition solution (Figure 2, plots b−d). At low concentration (0.01 mM), the intensities of the peaks at ~162 eV are greater than those at ~164 eV, which correlates with the high levels of bound thiolate for the associated SAMs revealed in Table S2 in the Supporting Information; however, at high concentration (1 mM), the intensities of the peaks at ~162 eV are less than those at ~164 eV, which indicates a significant reduction in bound thiolate for these SAMs as compared to those formed from the low concentration deposition solutions. The results for all SAMs formed at intermediate concentration (0.1 mM) fall in-between the two concentration extremes for each type of bidentate SAM. These data indicate that most of the sulfur moieties in the bidentate initiator monolayers formed at low concentration (0.01 mM) were bound to gold, but a large number of sulfur species present in the radical initiator monolayers formed at high concentration (1 mM) were unbound. A quantitative analysis of these data is discussed in the following paragraph. In contrast, we observed no strong influence of concentration on changes in the XPS S 2p spectra for the "monodentate" initiator monolayers (see Figure 2a), with adsorbate **M** giving rise to initiator monolayers with mostly bound thiol headgroups regardless of concentration. Additionally, we observed no peaks associated with oxidized sulfur species (>166 eV) in the S 2p region of the X-ray photoelectron spectra for the initiator monolayers generated from both **M** and the bidentate adsorbates (**B16**, **B10**, and **B4**).[14,36]

For quantitative analysis of the polymer initiator monolayers formed on gold surfaces, the percentages of bound thiolate were evaluated by deconvolution of the peaks in the S 2p region of the X-ray photoelectron spectra (see Figure S8 and Table S2 in the Supporting Information). Additionally, the relative adsorbate densities were determined using sulfur-to-gold (S/Au) ratios derived from the integrated peak areas for the S 2p and Au 4f binding energies (see Table S3 in the Supporting Information).[37,38] These results provide useful insight into the conformation of the adsorbates in the radical initiator monolayers depending on the concentration of the

DOI: 10.1021/acsami.6b02025
ACS Appl. Mater. Interfaces 2016, 8, 15691−15699

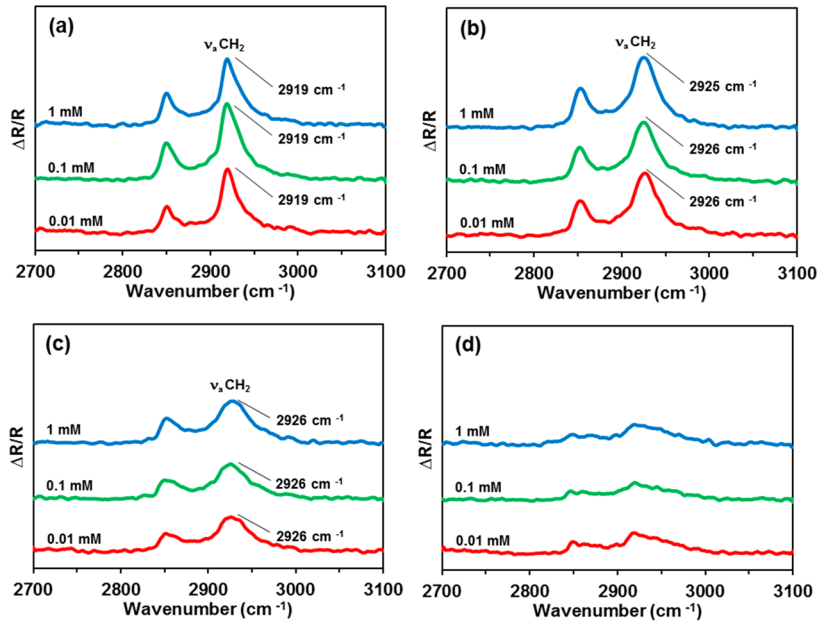

Figure 4. PM-IRRAS spectra of the C−H stretching region for the films generated at 0.01, 0.1, and 1 mM from (a) **M**, (b) **B16**, (c) **B10**, and (d) **B4** in THF.

initial adsorbate deposition solution. Figure 3a shows the changes in the percentages of bound thiolate as a function of concentration. For the initiator monolayer generated from **M**, there was only a 4% reduction in the amount of bound thiolate as the concentration of **M** in the deposition solution was increased from 0.01 to 1 mM. In contrast, a large decrease in the percentage of bound thiolate is apparent in the plots for the bidentate radical monolayers (**B16**, **B10**, and **B4**) upon increasing the concentration of the adsorbates in solution. Interestingly, differences in the percentages of bound thiolate between the films formed from the two concentration extremes (0.01 and 1 mM) depend strongly on the number of methylene units in the bidentate adsorbates; decrements in the percentages of bound thiolate for **B16**, **B10**, and **B4** were 45%, 27%, and 19%, respectively. Collectively, these results indicate that the percentages of bound thiolate were strongly influenced by the molecular length of the adsorbates as well as the type of headgroup (monodentate vs bidentate). Contrary to the trends associated with the percentage of bound thiolate, the relative densities of the adsorbates on the gold surfaces increased when the concentration of the adsorbate in solution increased (Figure 3b). Notably, the relative adsorbate density of the film formed from **B16** at 1 mM concentration was twice that at 0.01 mM. Furthermore, the relative adsorbate density of **B16** at 0.01 mM corresponds well with a theoretical relative density for the bidentate initiator adsorbates (i.e., 25%), assuming a model in which our α,ω-difunctional adsorbates with bidentate headgroups bind to gold with all four sulfur atoms relative to a conventional monodentate **C18SH** SAM at 100% adsorbate density. The differing trends in the data in Figure 3b for the monodentate adsorbate **M** compared to the bidentate adsorbates **B16**, **B10**, and **B4** are discussed in a later section.

Ellipsometric Thicknesses of Radical Initiator Monolayers. The ellipsometric thicknesses of the films formed from the bidentate adsorbates (**B16**, **B10**, and **B4**) increased linearly with an increase in the concentration of the adsorbate deposition solutions (see Figure 3c). However, the thicknesses of **M** showed a slightly different behavior, increasing by 6 Å when the concentration increased from 0.01 to 0.1 mM, but failing to show a significant change when the concentration was increased from 0.1 to 1 mM. This trend is similar to that found with the relative adsorbate densities (Figure 3b). Thin radical initiator films generated from the bidentate adsorbates (**B16**, **B10**, and **B4**) at low concentration (0.01 mM) exhibited low adsorbate densities, while thick films generated at high concentration (1 mM) had high adsorbate densities. These phenomena associated with the different types of radical initiator adsorbate are discussed in detail in a subsequent section.

PM-IRRAS Analysis of Radical Initiator Monolayers. An estimation of the conformational order (or "crystallinity") of the aliphatic chains in a SAM can be obtained from the band position of the antisymmetric methylene C−H stretching vibration ($\nu_a^{CH_2}$) measured using polarization modulation infrared reflection−absorption spectroscopy (PM-IRRAS).[39] Figure 4 provides the PM-IRRAS spectra for the four series of monolayer films, with three of the films yielding interpretable results regarding the relative conformational order of the radical initiator monolayers. The band positions for $\nu_a^{CH_2}$ for the films generated from the monodentate adsorbate (**M**) all appear at 2919 cm^{-1}, but the films generated from the two bidentate adsorbates (**B16** and **B10**) with the longer methylene chains appear at 2925−2926 cm^{-1}. These results indicate that the methylene units in the monolayers derived from **M** were more ordered than those in the monolayers derived from **B16** and **B10**. Interestingly, the PM-IRRAS data for the initiator monolayers generated from each adsorbate appear to be unaffected by the concentration of the adsorbate deposition solutions used in this study. These results can be rationalized as follows: when the α,ω-difunctional adsorbates form monolayers at low concentration (0.01 mM), they utilize both dithiol headgroups, producing optimal packing arrangements for their alkyl spacers, albeit at low adsorbate surface coverage. However, at higher adsorbate surface coverage (0.1 mM), the more highly

DOI: 10.1021/acsami.6b02025
ACS Appl. Mater. Interfaces 2016, 8, 15691−15699

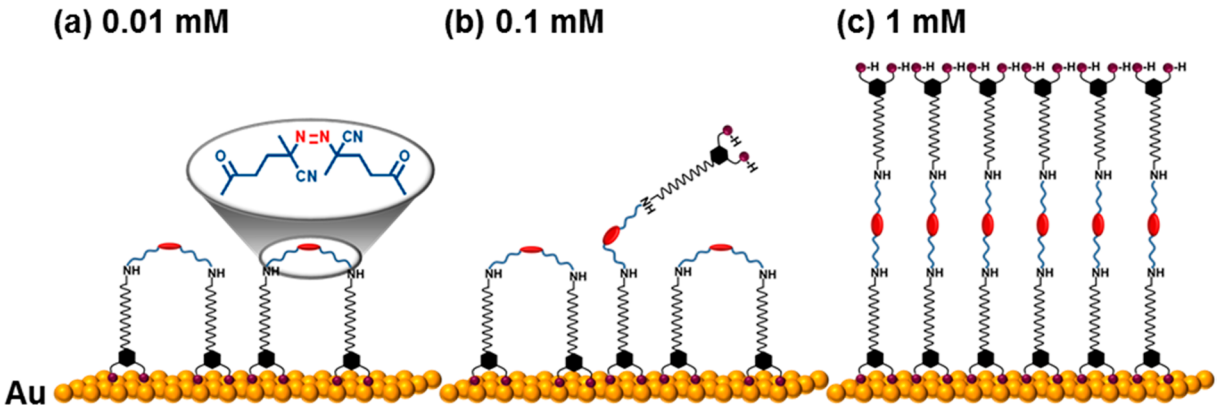

Figure 5. Schematic representation of the conformation of the **B16** adsorbates within monolayers generated from three different concentrations (0.01, 0.1, and 1 mM) of **B16** solution. (Note: these illustrations are provided to convey the general concepts for the organization of the monolayer films. Structural details such as the alkyl chain alignments have been drawn in their simplest form and do not reflect the conformational ordering indicated by the PM-IRRAS data.)

packed adsorbates likely form domains where the erect, but unbound, segment again produces optimal packing for the upper alkyl spacers. Also, at the highest concentration (1 mM), both the upper and the lower alkyl spacers are left with no option but to pack as efficiently as possible in an erect orientation. On the basis of this model, it is plausible that there is no discernible difference in the relative conformational order of the films generated at the different concentrations. Furthermore, any differences in the $\nu_a^{CH_2}$ band positions for the SAMs derived from the monodentate (**M**) versus the bidentate (**B16** and **B10**) adsorbates likely arise from the differences in their headgroups.[37] In addition, the bands for the antisymmetric methylene C−H stretching vibration ($\nu_a^{CH^2}$) of the monolayers formed from **B4** show significantly lower intensities (Figure 4d) due to the limited number of methylene units in the **B4** adsorbate.

Overall, on the basis of the results obtained from XPS, ellipsometry, and PM-IRRAS, we can summarize several noteworthy trends for the radical initiator monolayers generated from the monodentate (**M**) and bidentate (**B16**, **B10**, and **B4**) adsorbates. First, the structural parameters (film thickness, adsorbate density on the gold surface, and bound vs unbound sulfur) were influenced by the concentration of the adsorbate solutions. Second, the impact of concentration on the bidentate monolayers was markedly greater than that for the monodentate monolayers. Third, the effect of concentration on monolayer development increased with the chain length of the bidentate adsorbates (**B16** > **B10** > **B4**). Importantly, these three trends can be rationalized by entropic effects during the process of self-assembly for the monolayers, where low adsorbate concentrations afford low initial adsorbate densities that entropically favor multidentate binding (i.e., hairpin rather than standing-up structures). This phenomenon can be further illustrated by considering a simpler chelating ligand such as ethylenediamine; Cotton and Harris concluded that the superior stability of diamine-based chelate complexes could be attributed largely to entropy and suggested that a component of the stabilization arising from diamine ligands of different chain lengths was associated with the time to achieve ring closure.[40,41] Therefore, any delay in the bonding of an unbound end of a chelating compound owing to an increase in distance (i.e., chain length) reduces the likelihood of the formation of the chelate structure. Fourth, all of the bidentate adsorbates formed monolayers with high percentages of bound thiolate (≥94%), low adsorbate density (16−26%), and low film thickness at the lower deposition solution concentration (0.01 mM). In contrast, the bidentate adsorbates formed monolayers with low percentages of bound thiolate (≤75%), high adsorbate density (26−49%), and thicker films at the higher deposition solution concentration (1 mM). Using these experimental results and previous results reported by Kim and Gorman,[42] we drew models to depict the various conformations of the adsorbate chains for the **B16** monolayers generated at different concentrations (see Figure 5). At low concentration (0.01 mM), the adsorbates adopt a hairpin conformation to bind on gold with all four sulfur atoms. At high concentration (1 mM), however, the adsorbates adopt a standing-up conformation. Meanwhile, the hairpin and standing-up conformations coexist for the intermediate concentration (0.1 mM).

Interestingly, the monodentate adsorbate **M** exhibited a different behavior as a function of deposition solution concentration (see Figure 3a−c). Adsorbate **M** formed monolayers with similar percentages of bound thiolate (90%, 90%, and 86%) at the three different concentrations examined (0.01, 0.1, and 1 mM, respectively). Further, the relative adsorbate density and the film thickness for the **M** monolayer were saturated at 0.1 mM concentration, and the relative adsorbate densities of **M** at 0.1 and 1 mM are the same within experimental error (53% and 52%, respectively) and remarkably close to the maximum theoretical relative density for the α,ω-difunctional monodentate-thiol initiator adsorbates (i.e., 50%). We interpret these results to indicate that the monodentate adsorbate **M** adopts only a hairpin conformation to bind to gold at the concentrations employed in this investigation. The differing trends in behavior can be rationalized on the basis of the differing character of the monodentate versus bidentate headgroups. Upon making contact with the gold surface, the bidentate adsorbates bind strongly with little or no reversible desorption and lateral diffusion on the surface. Therefore, the surface conformation of the bidentate adsorbates depends largely on the concentration of the deposition solution (i.e., low concentrations give hairpins while high concentrations give standing-up conformations). In contrast, the monodentate adsorbate can readily undergo desorption and exchange with adsorbates in solution as well as diffuse laterally on the surface with relative ease.[43,44] Therefore, the initial concertation of **M**

DOI: 10.1021/acsami.6b02025
ACS Appl. Mater. Interfaces 2016, 8, 15691−15699

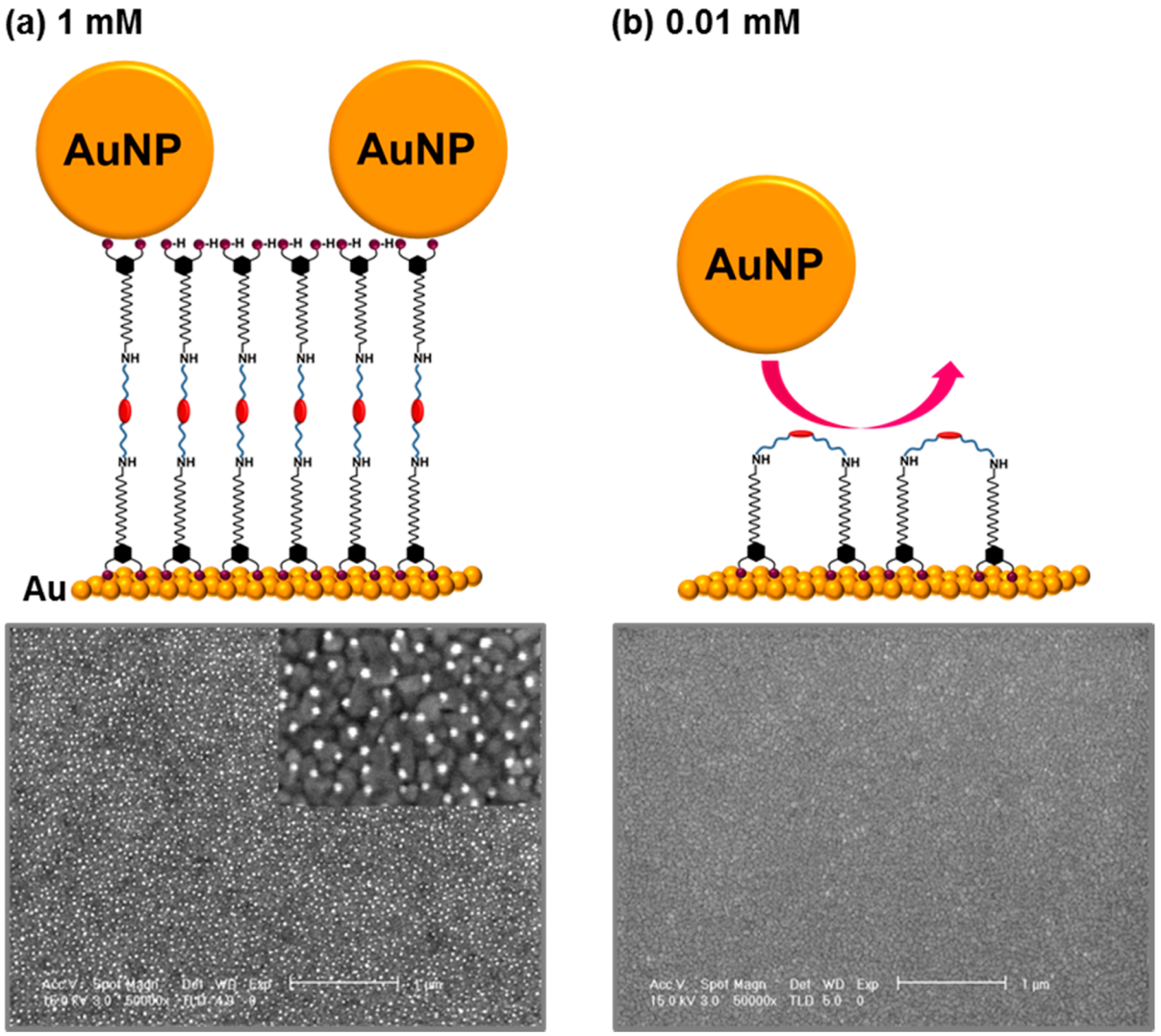

Figure 6. Illustrations and scanning electron microscopy (SEM) images of the gold nanoparticle (AuNP) interactions with the radical initiator monolayers generated from **B16** at (a) 1 mM and (b) 0.01 mM adsorbate concentrations. The scale bar on the images is 1 μm in length.

in the deposition solution can plausibly have comparably less of an impact on the conformation of **M** on the surface of gold.

To provide support for our model of bidentates, we conducted immobilization experiments using gold nanoparticles (AuNPs) on radical initiator monolayer surfaces generated from **B16** at two different concentrations (0.01 and 1 mM). After immersing the monolayer film-coated slides in aqueous solutions of citrate-stabilized AuNPs (size = ~30 nm) for 12 h, the resulting surfaces were analyzed by scanning electron microscopy (SEM). Regularly dispersed AuNPs were found on the **B16** monolayer developed at the higher concentration (1 mM) (Figure 6a). However, the surface of the **B16** monolayer that developed at the lower concentration (0.01 mM) was devoid of AuNPs after washing with deionized water (Figure 6b). These results can be interpreted to indicate that the AuNPs attach to the **B16** monolayers developed at 1 mM concentration due to the presence of unbound free thiols on these surfaces; in contrast, no AuNPs attach to the **B16** monolayers developed at 0.01 mM concentration due to the absence of unbound free thiols on these surfaces.

II. Thermal Stability of Radical Initiator Monolayers on Gold Surfaces. To evaluate the relative stability of the monolayers formed from **M**, **B16**, **B10**, and **B4** during thermally activated radical polymerization at elevated temperatures, we performed solution-phase thermal desorption tests as described in a previous report.[37,45] The radical initiator monolayers developed at low concentration (0.01 mM) were used for conducting these tests. In an initial set of experiments, we used ellipsometric thickness measurements to determine the average amount of adsorbate remaining after prolonged heating at 90 and 110 °C in a large excess of the nonpolar solvent decalin (decahydronapthalene). Figure 7 demonstrates the remarkable difference in thermal stability between the bidentate films (**B16**, **B10**, and **B4**) and the monodentate film (**M**). At the initial elevated temperature setting (90 °C, Figure 7a), while more than 80% of the bidentate adsorbates (**B16**, **B10**, and **B4**) remained on the surface after 90 min, less than 30% of the monodentate adsorbates (**M**) in the monolayers remained under the same conditions. At a higher temperature setting (110 °C, Figure 7b), while more than 60% of the bidentate adsorbates (**B16**, **B10**, and **B4**) remained on the surface after 90 min, most of the monodentate adsorbate (**M**) in the monolayers desorbed from the gold surfaces after 15 min. Interestingly, the thermal stability of the three bidentate adsorbates (**B16**, **B10**, and **B4**) appeared to be similar. These results can be interpreted to indicate that the initiator films

DOI: 10.1021/acsami.6b02025
ACS Appl. Mater. Interfaces 2016, 8, 15691−15699

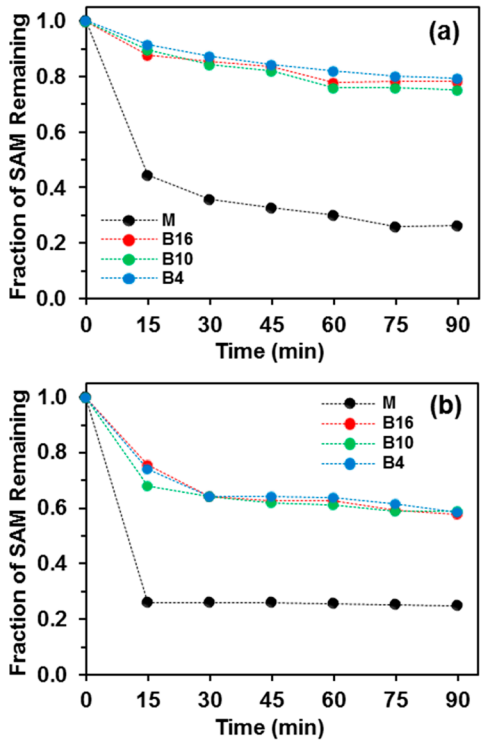

Figure 7. Solution-phase thermal desorption profiles of the indicated radical initiator monolayers in decalin as a function of time at (a) 90 °C and (b) 110 °C.

derived from **B16**, **B10**, and **B4** are markedly more stable than that derived from **M**. Furthermore, the chelate effect associated with the bidentate headgroup plays a more important role than the van der Waals forces associated with the interaction between the adsorbate chains for enhancing thermal stability in these radical initiator monolayer systems.[33,34,37,45]

III. Growth of Polymer Films from Radical Initiator Monolayers on Gold Surfaces. To evaluate the potential of the new radical initiator monolayers as platforms for surface-initiated polymerization, we performed a comparison study between the monolayers formed from the **M** and **B16** adsorbates by examining the thermal polymerization of polystyrene in toluene at 90 °C. We monitored the ellipsometric thicknesses of the developing polystyrene films formed on gold substrates as well as the peaks in the PM-IRRAS spectra associated with the C═C double bond stretching vibrations (1450, 1500, and 1600 cm^{-1}) for the aromatic moieties of polystyrene as a function of time.[31] As shown in Figure 8a, the thickness of the polystyrene films grown from the **B16** initiator monolayers increased linearly during the radical polymerization, but the thickness of the films grown from the **M** initiator monolayers was nearly constant over the course of 12 h. Interestingly, the thickness of the polystyrene films grown from the **B16** initiator monolayers (~40 nm) was the same as that of the polystyrene films grown from the cross-linked radical initiator monolayers reported by Huang and co-workers.[23] Furthermore, no saturation (i.e., thickness maximum) is observed in the thickness profiles for the polystyrene films grown from the **B16** initiator monolayers. The absence of saturation is consistent with a model in which the initiator radicals on the surfaces are still active throughout the 12 h experimental window.[23,31] Notably, the PM-IRRAS spectra in Figure 8 provide further evidence of the substantial

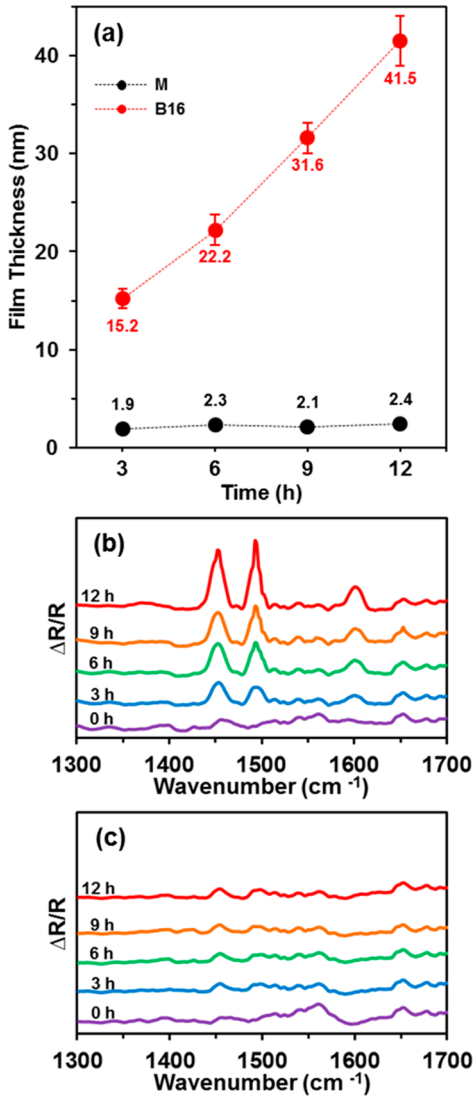

Figure 8. (a) Film thickness profiles of the polystyrene films generated from the indicated radical initiator monolayers on gold substrates as a function of time. PM-IRRAS spectra of the C═C double bond stretching region for the polystyrene films generated from (b) the **B16** monolayers and (c) the **M** monolayers on gold substrates as a function of time. Error bars indicate the standard deviation for the data.

difference in the effectiveness of the bidentate (**B16**) and monodentate (**M**) radical initiator films. The increase in intensity of the C═C double bond stretching vibrations at 1450, 1500, and 1600 indicate that polystyrene films were successfully generated from the **B16** initiator films (see Figure 8b). In contrast, no significant changes in intensity were observed for these vibrations in the PM-IRRAS spectra of the films generated from the **M** initiator (see Figure 8c). As a whole, these data provide further support for the efficacy of multidentate adsorbates for SAM generation[33,34,37,45] and illustrate a new, simple, and highly effective strategy for growing polymeric films on gold surfaces.

CONCLUSIONS

Custom-designed radical initiator adsorbates were synthesized to produce surface-bound polymer films on gold surfaces without the concomitant production of unbound polymeric material. Our new α,ω-difunctional thiol initiators (**B16**, **B10**,

DOI: 10.1021/acsami.6b02025
ACS Appl. Mater. Interfaces 2016, 8, 15691−15699

B4) possess bidentate character at both ends of their structures that circumvents problems associated with monodentate thiol initiators, such as thermal- and radical-induced desorption during the polymerization process.[23] The conformation adopted during surface bonding of these α,ω-difunctional thiol initiators depends on the concentration of the adsorbate in the deposition solution. At low concentration (0.01 mM), adsorbates **B16**, **B10**, and **B4** formed hairpin conformations on evaporated gold surfaces, yielding films with ≥94% of the sulfur atoms bound to gold. At high concentration (1 mM), however, these adsorbates formed standing-up conformations. Furthermore, the bidentate radical initiator adsorbates **B16**, **B10**, and **B4** showed enhanced thermal stability during the solution-phase thermal desorption tests when compared to the monodentate analogue **M**. As a consequence of the enhanced stability, polystyrene thin films were successfully grown on gold surfaces using the bidentate initiator monolayers. As such, these new bidentate radical initiator adsorbates offer a reliable strategy for growing polymers on flat and nanostructured surfaces, leading to new opportunities for polymer thin films as nanoscale coatings.

■ ASSOCIATED CONTENT

Supporting Information

The Supporting Information is available free of charge on the ACS Publications website at DOI: 10.1021/acsami.6b02025.

Supplemental data and detailed descriptions of the materials and synthetic procedures for preparing the adsorbates **B16**, **B10**, **B4**, and **M** along with the instrumental procedures used to conduct this research (PDF)

■ AUTHOR INFORMATION

Corresponding Author

*E-mail: trlee@uh.edu.

Notes

The authors declare no competing financial interest.

■ ACKNOWLEDGMENTS

We thank the National Science Foundation (CHE-1411265), the Robert A. Welch Foundation (Grant No. E-1320), and the Texas Center for Superconductivity at the University of Houston for generous support.

■ REFERENCES

(1) Hess, L. H.; Lyuleeva, A.; Blaschke, B. M.; Sachsenhauser, M.; Seifert, M.; Garrido, J. A.; Deubel, F. Graphene Transistors with Multifunctional Polymer Brushes for Biosensing Applications. *ACS Appl. Mater. Interfaces* **2014**, *6*, 9705−9710.

(2) Welch, M. E.; Ritzert, N. L.; Chen, H.; Smith, N. L.; Tague, M. E.; Xu, Y.; Baird, B. A.; Abruña, H. D.; Ober, C. K. Generalized Platform for Antibody Detection using the Antibody Catalyzed Water Oxidation Pathway. *J. Am. Chem. Soc.* **2014**, *136*, 1879−1883.

(3) Zhou, F.; Shu, W.; Welland, M. E.; Huck, W. T. S. Highly Reversible and Multi-Stage Cantilever Actuation Driven by Polyelectrolyte Brushes. *J. Am. Chem. Soc.* **2006**, *128*, 5326−5327.

(4) Zhou, F.; Biesheuvel, P. M.; Choi, E.-Y.; Shu, W.; Poetes, R.; Steiner, U.; Huck, W. T. S. Polyelectrolyte Brush Amplified Electroactuation of Microcantilevers. *Nano Lett.* **2008**, *8*, 725−730.

(5) Yang, L.; Sontag, S. K.; LaJoie, T. W.; Li, W.; Huddleston, N. E.; Locklin, J.; You, W. Surface-Initiated Poly(3-methylthiophene) as a Hole-Transport Layer for Polymer Solar Cells with High Performance. *ACS Appl. Mater. Interfaces* **2012**, *4*, 5069−5073.

(6) Whiting, G. L.; Snaith, H. J.; Khodabakhsh, S.; Andreasen, J. W.; Breiby, D. W.; Nielsen, M. M.; Greenham, N. C.; Friend, R. H.; Huck, W. T. S. Enhancement of Charge-Transport Characteristics in Polymeric Films Using Polymer Brushes. *Nano Lett.* **2006**, *6*, 573−578.

(7) Kitano, H.; Kondo, T.; Kamada, T.; Iwanaga, S.; Nakamura, M.; Ohno, K. Anti-Biofouling Properties of an Amphoteric Polymer Brush Constructed on a Glass Substrate. *Colloids Surf., B* **2011**, *88*, 455−462.

(8) Sin, M.-C.; Sun, Y.-M.; Chang, Y. Zwitterionic-Based Stainless Steel with Well-Defined Polysulfobetaine Brushes for General Bioadhesive Control. *ACS Appl. Mater. Interfaces* **2014**, *6*, 861−873.

(9) Jeong, S. P.; Lee, B. S.; Kang, S. M.; Ko, S.; Choi, I. S.; Lee, J. K. Binding Behaviors of Protein on Spatially Controlled Poly[oligo-(ethylene glycol)methacrylate] Brushes Grafted from Mixed Self-Assembled Monolayers on Gold. *Chem. Commun.* **2014**, *50*, 5291−5293.

(10) Rastogi, A.; Paik, M. Y.; Tanaka, M.; Ober, C. K. Direct Patterning of Intrinsically Electron Beam Sensitive Polymer Brushes. *ACS Nano* **2010**, *4*, 771−780.

(11) Sun, G.; Cho, S.; Clark, C.; Verkhoturov, S. V.; Eller, M. J.; Li, A.; Pavia-Jimenez, A.; Schweikert, E. A.; Thackeray, J. W.; Trefonas, P.; Wooley, K. L. Nanoscopic Cylindrical Dual Concentric and Lengthwise Block Brush Terpolymers as Covalent Preassembled High-Resolution and High-Sensitivity Negative-Tone Photoresist Materials. *J. Am. Chem. Soc.* **2013**, *135*, 4203−4206.

(12) Shah, R. R.; Merreceyes, D.; Husemann, M.; Rees, I.; Abbott, N. L.; Hawker, C. J.; Hedrick, J. L. Using Atom Transfer Radical Polymerization To Amplify Monolayers of Initiators Patterned by Microcontact Printing into Polymer Brushes for Pattern Transfer. *Macromolecules* **2000**, *33*, 597−605.

(13) Kaholek, M.; Lee, W.-K.; LaMattina, B.; Caster, K. C.; Zauscher, S. Fabrication of Stimulus-Responsive Nanopatterned Polymer Brushes by Scanning-Probe Lithography. *Nano Lett.* **2004**, *4*, 373−376.

(14) Schmidt, R.; Zhao, T.; Green, J.-B.; Dyer, D. J. Photoinitiated Polymerization of Styrene from Self-Assembled Monolayers on Gold. *Langmuir* **2002**, *18*, 1281−1287.

(15) Kaholek, M.; Lee, W.-K.; Feng, J.; LaMattina, B.; Dyer, D. J.; Zauscher, S. Weak Polyelectrolyte Brush Arrays Fabricated by Combining Electron-Beam Lithography with Surface-Initiated Photopolymerization. *Chem. Mater.* **2006**, *18*, 3660−3664.

(16) Schmelmer, U.; Paul, A.; Küller, A.; Steenackers, M.; Ulman, A.; Grunze, M.; Gölzhäuser, A.; Jordan, R. Nanostructured Polymer Brushes. *Small* **2007**, *3*, 459−465.

(17) Edmondson, S.; Osborne, V. L.; Huck, W. T. S. Polymer Brushes via Surface-Initiated Polymerizations. *Chem. Soc. Rev.* **2004**, *33*, 14−22.

(18) Hui, C. M.; Pietrasik, J.; Schmitt, M.; Mahoney, C.; Choi, J.; Bockstaller, M. R.; Matyjaszewski, K. Surface-Initiated Polymerization as an Enabling Tool for Multifunctional (Nano-)Engineered Hybrid Materials. *Chem. Mater.* **2014**, *26*, 745−762.

(19) Jones, D. M.; Brown, A. A.; Huck, W. T. S. Surface-Initiated Polymerizations in Aqueous Media: Effect of Initiator Density. *Langmuir* **2002**, *18*, 1265−1269.

(20) Bao, Z.; Bruening, M. L.; Baker, G. L. Rapid Growth of Polymer Brushes from Immobilized Initiators. *J. Am. Chem. Soc.* **2006**, *128*, 9056−9060.

(21) Zhou, F.; Zheng, Z.; Yu, B.; Liu, W.; Huck, W. T. S. Multicomponent Polymer Brushes. *J. Am. Chem. Soc.* **2006**, *128*, 16253−16258.

(22) Lv, B.; Zhou, Y.; Cha, W.; Wu, Y.; Hu, J.; Li, L.; Chi, L.; Ma, H. Molecular Composition, Grafting Density and Film Area Affect the Swelling-Induced Au-S Bond Breakage. *ACS Appl. Mater. Interfaces* **2014**, *6*, 8313−8319.

(23) Huang, W.; Skanth, G.; Baker, G. L.; Bruening, M. L. Surface-Initiated Thermal Radical Polymerization on Gold. *Langmuir* **2001**, *17*, 1731−1736.

(24) Saha, S.; Bruening, M. L.; Baker, G. L. Facile Synthesis of Thick Films of Poly(methyl methacrylate), Poly(styrene), and Poly(vinyl

DOI: 10.1021/acsami.6b02025
ACS Appl. Mater. Interfaces 2016, 8, 15691−15699

pyridine) from Au Surfaces. *ACS Appl. Mater. Interfaces* **2011**, *3*, 3042−3048.
(25) Liu, X.; Sun, K.; Wu, Z.; Lu, J.; Song, B.; Tong, W.; Shi, X.; Chen, H. Facile Synthesis of Thermally Stable Poly(*N*-vinylpyrrolidone)-Modified Gold Surfaces by Surface-Initiated Atom Transfer Radical Polymerization. *Langmuir* **2012**, *28*, 9451−9459.
(26) Ista, L. K.; Mendez, S.; Pérez-Luna, V. H.; López, G. P. Synthesis of Poly(*N*-isopropylacrylamide) on Initiator-Modified Self-Assembled Monolayers. *Langmuir* **2001**, *17*, 2552−2555.
(27) Park, H. H.; Lee, T. R. Thermo- and pH-responsive Hydrogel-Coated Gold Nanoparticles Prepared from Rationally Designed Surface-Confined Initiators. *J. Nanopart. Res.* **2011**, *13*, 2909−2918.
(28) Pinto, J. C.; Whiting, G. L.; Khodabakhsh, S.; Torre, L.; Rodríguez, A. B.; Dalgliesh, R. M.; Higgins, A. M.; Andreasen, J. W.; Nielsen, M. M.; Geoghegan, M.; Huck, W. T. S.; Sirringhaus, H. Organic Thin Film Transistors with Polymer Brush Gate Dielectrics Synthesized by Atom Transfer Radical Polymerization. *Adv. Funct. Mater.* **2008**, *18*, 36−43.
(29) Kitano, H.; Anraku, Y.; Shinohara, H. Sensing Capabilities of Colloidal Gold Monolayer Modified with a Phenylboronic Acid-Carrying Polymer Brush. *Biomacromolecules* **2006**, *7*, 1065−1071.
(30) Matyjaszewski, K.; Tsarevsky, N. V. Macromolecular Engineering by Atom Transfer Radical Polymerization. *J. Am. Chem. Soc.* **2014**, *136*, 6513−6533.
(31) Prucker, O.; Rühe, J. Polymer Layers through Self-Assembled Monolayers of Initiators. *Langmuir* **1998**, *14*, 6893−6898.
(32) Czaun, M.; Hevesi, L.; Takafuji, M.; Ihara, H. Novel Surface-Attachable Multifunctional Initiators: Synthesis, Grafting, and Polymerization in Aprotic and Protic Solvents. *Macromolecules* **2009**, *42*, 4539−4546.
(33) Park, C. S.; Lee, H. J.; Jamison, A. C.; Lee, T. R. Robust Thick Polymer Brushes Grafted From Gold Surfaces Using Bidentate Thiol-Based Atom-Transfer Radical Polymerization ATRP Initiators. *ACS Appl. Mater. Interfaces* **2016**, *8*, 5586−5594.
(34) Chinwangso, P.; Jamison, A. C.; Lee, T. R. Multidentate Adsorbates for Self-Assembled Monolayer Films. *Acc. Chem. Res.* **2011**, *44*, 511−519.
(35) Castner, D. G.; Hinds, K.; Grainger, D. W. X-ray Photoelectron Spectroscopy Sulfur 2p Study of Organic Thiol and Disulfide Binding Interactions with Gold Surfaces. *Langmuir* **1996**, *12*, 5083−5086.
(36) Duwez, A.-S. Exploiting Electron Spectroscopies to Probe the Structure and Organization of Self-Assembled Monolayers: a Review. *J. Electron Spectrosc. Relat. Phenom.* **2004**, *134*, 97−138.
(37) Lee, H. J.; Jamison, A. C.; Lee, T. R. Boc-Protected ω-Amino Alkanedithiols Provide Chemically and Thermally Stable Amine-Terminated Monolayers on Gold. *Langmuir* **2015**, *31*, 2136−2146.
(38) Gao, D. Q.; Scholz, F.; Nothofer, H.-G.; Ford, W. E.; Scherf, U.; Wessels, J. M.; Yasuda, A.; von Wrochem, F. Fabrication of Asymmetric Molecular Junctions by the Oriented Assembly of Dithiocarbamate Rectifiers. *J. Am. Chem. Soc.* **2011**, *133*, 5921−5930.
(39) Porter, M. D.; Bright, T. B.; Allara, D. L.; Chidsey, C. E. D. Spontaneously Organized Molecular Assemblies. 4. Structural Characterization of *n*-Alkyl Thiol Monolayers on Gold by Optical Ellipsometry, Infrared Spectroscopy, and Electrochemistry. *J. Am. Chem. Soc.* **1987**, *109*, 3559−3568.
(40) Schwarzenbach, G. Der Chelateffekt. *Helv. Chim. Acta* **1952**, *35*, 2344−2359.
(41) Cotton, F. A.; Harris, F. E. The Thermodynamics of Chelate Formation. 1. Experimental Determination of Enthalpies and Entropies in Diamine-Metal Ion Systems. *J. Phys. Chem.* **1955**, *59*, 1203−1208.
(42) Kim, Y.-H.; Gorman, C. B. Standing Up versus Looping Over: Controlling the Geometry of Self-Assembled Monolayers of α,ω-Diynes on Gold. *Langmuir* **2011**, *27*, 6069−6075.
(43) Love, J. C.; Estroff, L. A.; Kriebel, J. K.; Nuzzo, R. G.; Whitesides, G. M. Self-Assembled Monolayers of Thiolates on Metals as a Form of Nanotechnology. *Chem. Rev.* **2005**, *105*, 1103−1169.
(44) Stranick, S. J.; Parikh, A. N.; Tao, Y.-T.; Allara, D. L.; Weiss, P. S. Phase Separation of Mixed-Composition Self-Assembled Monolayers into Nanometer Scale Molecular Domains. *J. Phys. Chem.* **1994**, *98*, 7636−7646.
(45) Lee, H. J.; Jamison, A. C.; Yuan, Y.; Li, C.-H.; Rittikulsittichai, S.; Rusakova, I.; Lee, T. R. Robust Carboxylic Acid-Terminated Organic Thin Films and Nanoparticle Protectants Generated from Bidentate Alkanethiols. *Langmuir* **2013**, *29*, 10432−10439.

DOI: 10.1021/acsami.6b02025
ACS Appl. Mater. Interfaces 2016, 8, 15691−15699